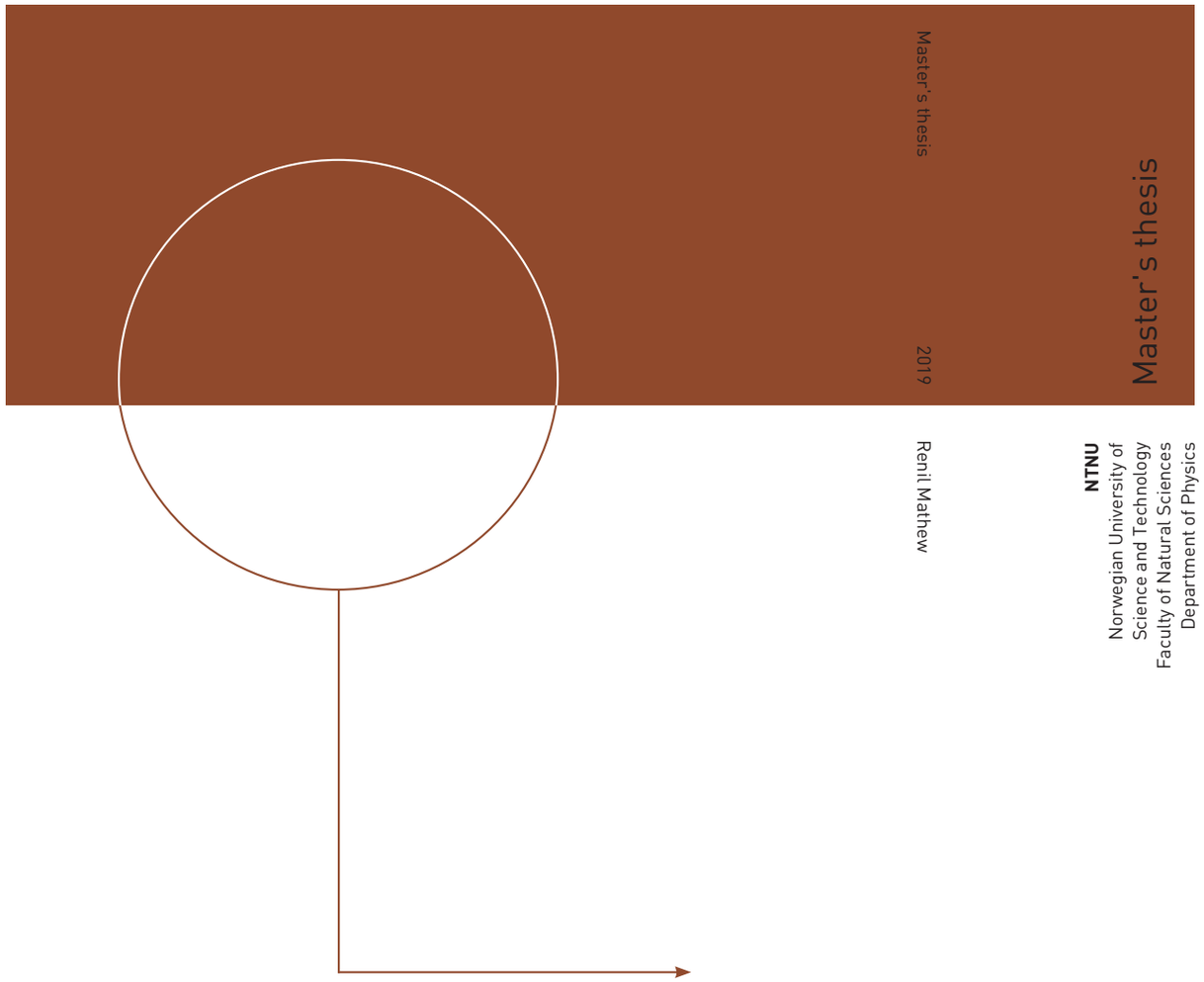

Master's thesis

2019

Renil Mathew

**NTNU**
Norwegian University of
Science and Technology
Faculty of Natural Sciences
Department of Physics

Renil Mathew

# Modeling hemodynamic responses during virtual navigation in human 7T- fMRI

August 2019

NTNU
Norwegian University of
Science and Technology

NTNU
Norwegian University of
Science and Technology

Master's Thesis in Physics
August 2019

# Modeling hemodynamic responses during virtual navigation in human 7T-fMRI


Thesis author : Renil Mathew
Project supervisor : Matthias Nau
Principle supervisor : Christian Doeller

Norwegian University of Science and Technology
Faculty of Natural Sciences
Kavli Institute of Systems Neuroscience





*dedication.*

To the creator of my dreams!

# Abstract

Functional magnetic resonance imaging (fMRI) is one of the most widely used non-invasive neuroimaging technique in humans. fMRI measures neural activity indirectly in the form of the blood-oxygen-level-dependent (BOLD) signal. This signal reflects hemodynamic fluctuations that are induced by neural population activity. Statistical analysis of the acquired data requires comparing the task-derived predictions of the BOLD signal to the one observed during the experiment. Typically, the predicted BOLD signal is modeled by convolving a hemodynamic response function (HRF) with the neural stimulus functions. The HRF shape represents the variation in BOLD signal in response to a neural event. Most fMRI studies assume a pre-defined canonical HRF. However, several earlier studies suggested that the HRF shows strong inter-subject and inter-regional variations that are not captured by the canonical HRF. Slight variations in the modeling of HRF could cause significant deviation from the predicted and observed BOLD signal, affecting the results and complicating subsequent interpretation of the data.

Here, we used 7T-fMRI in combination with virtual reality (VR) to study the shape of the HRF related to virtual navigation behavior. We assess the HRF in 18 participants across cortical and sub-cortical regions during a virtual navigation task. We estimate the HRF as a function of the navigation behavior (translations and rotations) using finite impulse response (FIR) basis sets in multilinear regression analysis. The flexibility of FIR acknowledges the variability of observed BOLD signals, allowing us to estimate the HRF without prior assumption about its shape. We then extracted the peak latency and the amplitude from the HRF of each voxel and compared it across regions involved in visual perception and navigation. We found differences in the HRF parameters across subjects and regions in line with previous work. Our predicted BOLD signal from showed higher correlation to the observed BOLD signal in some regions when compared to the frequently used canonical HRF.

# Acknowledgement

I would like to express my ineffable gratitude to Matthias Nau, for being an incredible mentor. His work ethic and dedication have immensely influenced my learning process during this project. He was always approachable to ask for guidance and knowledge. And to the question he never asked ”Could you work any harder?”, I will wholeheartedly answer ”Yes boss!”

My sincere thanks to Christian Doeller for giving me the opportunity to work with such a fun and motivated group of researchers. I would like to thank all the members of the Doeller group for maintaining a positive and social working environment. I’m thankful to Raphael Kaplan for offering guidance during the entire process. I’m much obliged to all my friends who have always being a support factor in my life. Especially to my friends in Trondheim, who have encouraged and helped me during this period.

Above all, I would like to thank my family for their love, care and support.

# Table of Contents

# List of Figures

# Abbreviations

| | | |
|---|---|---|
| Symbol | = | definition |
| HRF | = | Hemodynamic response function |
| fMRI | = | Functional magnetic resonance imaging |
| BOLD | = | Blood-oxygenation level dependent |
| VR | = | Virtual reality |
| FIR | = | Finite impulse response |
| EC | = | Entorhinal cortex |
| HC | = | Hippocampus |
| PHC | = | Parahippocampus |
| V1 | = | Visual cortex or Pericalcarine sulcus |
| CHRF | = | Canonical hemodynamic response function |
| GLM | = | General linear model |
| mse | = | Mean squared error |
| ROI | = | Region of Interest |
| SPM | = | Statistical parametric mapping |
| 3D EPI | = | Three dimensional echo-planar imaging |
| TR | = | Repetition time |
| SEM | = | Standard error of mean |

Chapter 1

# Introduction

The neural underpinnings of spatial navigation have been studied for decades, revealing the existence of a 'cognitive map' in the late 1940's by Tolman [1]. His results propose that the brain creates a unified representation of the spatial environment to guide memory and initiate future actions. In his experiment, rats who had learned a roundabout route to a goal were able to adapt and change to a more direct path if the previously learned route was obstructed. This observation helped to conclude the presence of a map-like representation of the environment , which the animal uses to navigate by taking shortcuts, which a route-based strategy would not.

Through the years, neurobiological discoveries have supported the development of cognitive maps. The pioneers of such discoveries were O'Keefe and Nadel [2], who found the place cells in the rat hippocampus that fire as a function of spatial position of the animal. Subsequent to this, various discoveries such as the grid cell (firing in hexagonal lattice, , which code metric distances)[3], head direction cells(tracking head direction)[4] and border cells(tracking the distance to a boundary)[5] have shaped a model system that encodes navigation related quantities , which in turn helped us understand how the brain process high level cognitive functions.

Non-invasive neuroimaging methods have helped us study these complex systems in humans. Functional magnetic resonance imaging (fMRI) is currently the mainstay in human neuroimaging with relatively high spatiotemporal resolution and capacity to map the entire network of brain regions during an experimental task. Introducing virtual navigation experiments in fMRI have allowed us to study naturalistic navigation mechanisms. These studies have shown map-like[6] and grid-like[7] [8] representation in different brain regions suggesting a similar mechanism in humans.

However, most of these fMRI studies assume a specific relationship between neural activity and the evoked fMRI signal. Evidences from various basic fMRI studies show that this assumed relationship might not be accurate. Here we test this relationship in the context of spatial navigation in humans.

## 1.1 Functional magnetic resonance imaging

Functional magnetic resonance imaging (fMRI) is a widely used non-invasive technique that helps us study human brain functions. Functional MRI is an extension of magnetic resonance imaging , which provide additional information about biological function alongside the anatomical information. The activity of neurons within a brain region is coupled to the increase in cerebral blood flow to that region, , which is often called as the neurovascular coupling [9]. Functional activation of the brain corresponds to this neurovascular coupling . By measuring the blood- oxygenation-level-dependent (BOLD) signal we measure the brain activity by detecting the signal variation as a result of increased blood oxygenation[10]. This proxy signal reflects neuronal mass activity of different brain regions. The presence of deoxyhemoglobin (dHb), which is paramagnetic, influences the MR signal negatively. Upon neural activation the variation in blood oxygenation causes increase or decrease in the BOLD signal. This signal variations give the contrast to the fMRI images we acquire. The critical factors that help us make conclusions from these brain images depends on the signal strength and spatio - temporal resolution. The generated images should have high signal strength, reflecting the actual neural responses to events. The degree of spatial and temporal resolution helps us distinguish elementary units of activated regions and the time course of various neural changes respectively[11]. The BOLD signal variation for a neural event is characterised by the hemodynamic response function (HRF) , which helps us translate a neural response to the respective vascular response.

## 1.2 Hemodynamic response function (HRF)

Hemodynamic response (HR) is a term coined to relate the MR signal triggered by a neural activity. The basic goal of fMRI is to find the correlation between the BOLD response and stimulus to make

conclusions about the neural activation. The function that explains the variation of BOLD signal in response to a stimulus is called Hemodynamic response function (HRF). HRF modeling conducted in most studies helps us get a potential measure of response magnitude, latency and duration of neuronal activity.

Studying the shape of estimated HRF by measuring the response height, time-to-peak and full-width at half-maximum can be used to infer information about the intensity, time to peak amplitude and duration of the underlying hemodynamic response. The precise timing and waveform of the hemodynamic function helps researchers infer about the relative timing of neural activity, neural feedback events, and sustained activity of a brain region.[11]

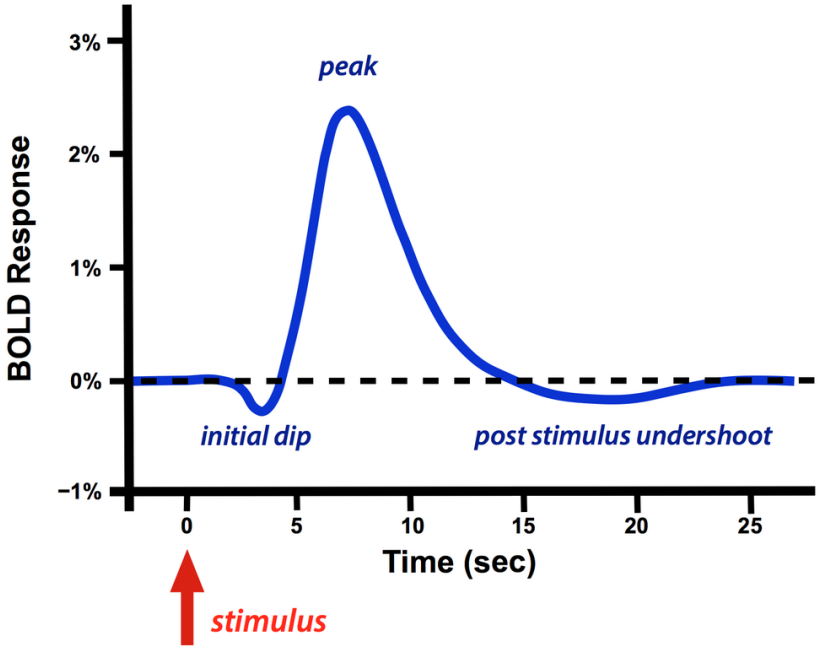


**Figure 1.1:** Hemodynamic response function: Typical Hemodynamic response function characteristics showing the initial dip, the peak and post stimulus undershoot. [adapted from [12]]

A hemodynamic response function has three major characteristics: initial dip, peak and an undershoot, which I will describe in detail in the following:

### Initial dip

The function characterise an initial dip in response to a stimulus. The transient energy demand due to neural activity result in decrease in the oxygenated hemoglobin (Hb) in the respective neural

region. This increases the deoxygenated Hb level, which in turn results in decreased MR signal. The dip is seen within 1-2 seconds after the stimulus. In some of the HRF models, the initial dip is ignored due its rare detection without finer temporal resolution of MR signal.

**Peak**

Subsequent to the dip, the function ramps to a peak value in a few seconds. Due to a sudden decrease in oxygenated blood in the responsive region, blood flow towards the region is increased to provide with more oxygen. This increases the MR signal. The MR signal keeps increasing until it reaches a peak value and the maximum amplitude is achieved around 4-6 seconds after the stimulus.

**Post stimulus undershoot**

After the peak amplitude is achieved, the function shoots down to baseline. The MR signal drops rapidly to reach the baseline around 16 seconds and then it further goes below the baseline. The BOLD response rises gradually to the a baseline activity for a sustained period of time. The accurate mechanism for this post stimulus undershoots remains unclear. It likely is due to a) sustained cerebral metabolic rate of oxygen b) post activation reduction in cerebral blood flow and c) delayed change in cerebral blood volume[13].

## 1.3 HRF and Data analysis

The neural responses to a stimulus is mostly instantaneous. A disadvantage as mentioned before, the fMRI signal acquired is a surrogate signal. The neural response to a stimulus and the acquired BOLD response is delayed by 4-6 seconds. To match the time courses of neural response and the time course of the BOLD signal, the stimulus function is convolved with a pre-specified hemodynamic response function[14], assuming it to be a linear time invariant system[15]. This convolved function is considered as a predicted BOLD signal time series. The predicted BOLD signal is then used to explain the variability in the observed BOLD signal mostly using a general linear model approach. Therefore, using an inaccurate HRF gives an inaccurate reflection of brain response to a stimulus, which can question the validity of follow-up statistical analysis.

The exact interpretability of an evoked BOLD response is complex, for instance; the neural response to a repeated stimulus can vary over time during a experiment. Also, the duration of the neuronal activity result in integration of the hemodynamic response across time giving an increased amplitude and duration to the BOLD signal. Another factor that could affect the BOLD signal is the saturation of the vascular response over time. These complex relationship between the neural activity and the evoked BOLD response is not clear to date. In spite of this, studies have treated the BOLD response as the signal of interest by adding them linearly and using smooth functions to model a HRF[14].

In most studies the variability in HRF across participants and regions is assumed to be minimal and all neural events is assumed to evoke a fixed shaped HRF. However, studies have shown that this assumption is not right even on a simple sensorimotor task [16], showing significant variation in HRF shape across participants in primary motor cortex. Furthermore, HRFs seem to have variation in amplitude and time-to-peak between regions within a single participant [17]. There are multiple factors that cause this inter-subject and inter-region variability in the shape of HRFs. The neural activity differences, partial volume imagining of veins, slice timing differences, global magnetic susceptibilities, vasculature differences, pulse differences, caffeine, alcohol and baseline cerebral blood flow [18] [19] [20] [21] are few of them. A statistical study that compared an empirically derived HRF to a commonly used canonical HRF shows that a misestimation as small as 1 second in the time-to-onset affected the model parameter estimation.[22]. In summary, studies have shown the variability in HRF and the potential negative effect of assuming HRF consistency across participants and brain regions. Therefore, a precise estimation of evoked HRF plays a crucial role in correct interpretation of neuroscientific studies based on fMRI data.

## 1.4 Aim and rationale

Relaying on the results from previous studies, it is evident that the hemodynamic response function varies across participants and brain regions[16][23]. Assuming a consistent HRF during data analysis have given results, but in most cases causing assessing bias and power-loss. Currently used HRF models are generally estimated based on studies from cortical regions like visual cortex or motor-sensory cortex. The vasculature, firing mechanism and functions are drastically different

across regions, questioning the use of these models in higher cognitive studies that mainly focus on subcortical brain structures

From the BOLD fMRI data acquired in the quest for studying cognitive maps involved in navigation during a object-location memory task, we used a finite impulse response model (FIR) to estimate the true HRF for navigation onsets. The estimated HRF is used to extract the amplitude and delay to peak (sec) values. The extraction is carried out by curve fitting the estimated HRF with different canonical HRF kernels that vary in its delay to peak(sec) values. In addition, to test if the FIR modelled HRFs outperform the canonical HRF in terms of predictability, we split the data into training and test runs. The training run is used to estimate the FIR based HRF. The estimated model from the training runs is convolved with the evoked BOLD signal of the test runs. The estimated model is then compared to the commonly used canonical HRF. Furthermore, we suggest ways to make the simulations better to reduce power-loss due to bias in modeling.

Chapter 2

# Theory and Methods

This chapter is divided into five section. The first section (1) includes the details of the data acquisition and the experimental design. The general outlook of fMRI data and the preprocessing steps are also mentioned in the first section. The second part (2) of the chapter covers the first level analysis steps including the theory behind the applied concepts that led to the estimation of the HRF. Section 3 explains the method used for extracting parameters from the estimated HRF. The following section (4) discusses statistical inferences carried out using the estimated HRF and their parameters. In the final section (5), we compare the efficiency of the extracted HRF model to the commonly used canonical HRF model .

## 2.1 Experiment

### 2.1.1 Data acquisition

The data analysed here have been used in previous work [24]. Twenty six participants (11 females, age 19-36, mean 23 years) performed a virtual navigation task while brain activity was monitored using 7T-fMRI. Out of the 26 participants 4 were removed from the analysis due to excessive movement that exceeded the mean plus 1 standard deviation (number of instantaneous movements)[25]. In addition, another 4 participants were excluded for technical reasons or if they had fewer than 4 scanning runs. In total, 18 participant entered our analysis.

Blood-oxygenation-level-dependent(BOLD) T2* weighted functional images were acquired on a 7T Siemens MAGNETOM scanner using a three dimensional echo-planar imaging (3D EPI) pulse

sequence [26] on a 32-channel surface coil: TR = 2.7 s, TE = 20 ms, flip angle = 14, slice thickness = 0.92 mm, slice oversampling = 8.3 %, in-plane resolution = 0.9∧ 2 mm, field of view (FoV) = 210 mm in each direction, 96 slices, phase encoding acceleration factor= 4, 3D acceleration factor= 2. The first five volumes of the main scan were discarded to allow for T1 equilibration. A field map using a gradient echo sequence was recorded for distortion correction of the acquired EPI images.

### 2.1.2 Experimental Design

The navigation task performed by the participants was an object-location memory task (Fig.2.1) while freely navigating in a virtual environment, a task adapted from Doeller and colleagues[27]. The participants collected and replaced six everyday objects within a virtual arena in their own pace. They collected all objects from its associated location once during an initial trial, by running over it. In the next trial they saw an image (cue) of one of the objects in the upper part of the screen and had to move to the object's associated location and press a button. Once the button is pressed, the object appeared at its associated position and participants collected it again. After an average of 3 trials/runs (ranged 2-4 trials), a fixation cross on a gray background was presented for 4 seconds (intertrial-interval,ITI). Each scanning session was subdivided into EPI acquisition blocks of 210 volumes. Participants had a maximum of 5 runs and the average per participant was less than 5.

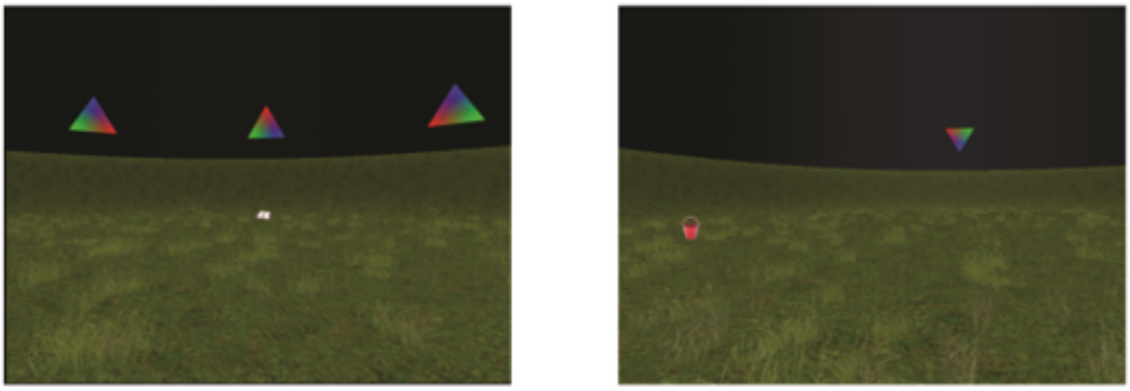

**Figure 2.1:** Virtual Reality environment, in which participants performed a self-paced object-location memory task. [Image adapted from [24]]

### 2.1.3 Preprocessing

Preprocessing steps assures that the assumptions of the analysis are met. Preprocessing makes sure that the time course comes from a single location and is uniformly spaced in time. There are numerous physical influences on the signal, which make the analysis of fMRI data a complex process. The analysis helps to separate noise from the data. The data undergo several preprocessing steps before entering statistical analysis. For this project we used an already preprocessed data. All the steps were carried out in a specific pipeline within different software toolboxes included in SPM, FSL and ANTs. Below we will discuss the preprocessing steps:

a)Motion correction: removing noise from respiration, head motion etc; b)Unwarping: mapping and correcting magnetic field distortions; c)Slice-time correction: aligning the slices acquired in one TR by phase shifting; d)Coregistration: aligning the structural scan to the functional scans. e)Normalization: transforming each participant's brain anatomy into a standardized space; f)Segmentation: creating a tissue segmentation mask based on intensity and anatomical locations; g)Spatial smoothing: smoothing each voxel with weighted average of itself and its neighbours. h)High-pass filtering: to fix the mean-signal intensity drift over time[28].

The preprocessed data is used for further data analysis. The characteristics of fMRI data and tools used here are explained in the following section.

### 2.1.4 fMRI data

The fMRI data is acquired as a four dimensional data file (3 x space and 1 x time), which correspond to the BOLD signal of the brain over time. The data file is a sequence of three dimensional functional volumes of brain images compiled together in time to give a 4D file. A single brain image is modelled as thousands of cubes or "voxels" of specific volume. Our data had 1328354 voxels per participant. Another view of looking at the acquired 4D data is as a time course of individual voxels. The BOLD signal varies in the brain areas in response to the experimental task and the basic fMRI task analysis help identify these activated locations.

In this project, the fMRI data analysis was carried out using the well-established Statistical parametric mapping (SPM) toolbox [14] implemented in Matlab. SPM help us to create different processed images where each voxel is analysed using univariate statistical parametric tests. The

assembly of voxels are considered as an image constructed by spatially extended statistical processes which help us to test hypotheses neurobiological effects on the regions we are interested in. The wide application of SPM is mainly due to its simplicity and success in diverse experimental paradigms. In SPM, the analysis can be divided into two major steps. The first level analysis and the second level analysis, which correspond to participant-wise analysis and group level analysis respectively.

## 2.2 First level-data analysis

The first level data analysis refers to single participant statistical testing. We conduct different steps to extract interested information from each individual participant. We use the General linear model (GLM) analysis which is widely used in fMRI studies for modeling and statistical testing. In this section you will find how we modelled the variables of interest and how we defined the finite-impulse response (FIR) basis sets to create a design matrix for the GLM analysis. The section also includes basic theory necessary to understand the analysis.

### 2.2.1 General linear model (GLM)

The general linear model (GLM) is the most widely used technique for analysing task-based fMRI experiments. The analysis helps us model the observed signal/data(Y) in terms of a single or multiple explanatory variables. These variables are often known as regressors(X). Regressors are the hypothesised variables of interest that could have affected the observed experimental data. The regressors can be flickering checker boards, image cues, button presses, etc; which are included at known or extractable time points during a experiment. The analysis scales these regressors and linearly combine them together to give the best explanation of the data. The best scaling parameter ($\beta$) is determined by finding the least residual error ($\varepsilon$)(least squared error), which is a measure of the difference between the actual data and the scaled regressor model ($X\beta$) (equ. 2.1). GLM's can involve the use of time series and multiple regressors but the linearity in the model remains in how the one type of regressor is combined together to explain the data. When we have multiple

regressors for analysing the data, it is called as multi-linear regression (Fig.2.4).

$$Y = X\beta + \epsilon \tag{2.1}$$

### 2.2.2 GLM for fMRI data

The fMRI data is a time-series data which can be analysed using GLM. The analysis in most cases involve more than one regressor, hence called a multi-linear regression. The regressors in fMRI analysis are modelled differently by convolving the regressor function with a HRF to translate the neural responses to vascular responses, which is explained below.

#### HRF-convolution

The neural responses are a lot quicker than the change in blood flow. The neuronal activity triggers a hemodynamic change with a certain latency typically assumed to be around 6 seconds. To study the observed BOLD signal we need to synchronize it to corresponding regressors. The regressors as mentioned earlier are variables that could have affected the BOLD signal. To create a regressor that matches the hemodynamic activity the regressors are convolved with a HRF (Fig.2.2). The convolution helps us transform the neural stimulus regressors into vascular response regressors [15], hence giving a prediction of the expected BOLD signal. Incorrect modeling of HRF might cause significant variance in GLM coefficents, power and model validity [16][29]. Many models have been proposed with various degrees of freedom to account for the variability in the evoked BOLD signal[11]. Most of fMRI studies use a fixed shape (canonical HRF model) by ignoring the variability in HRF shape. At the top of the flexibility spectrum is the finite impulse response (FIR) basis sets, which is used in this project to estimate the true HRF for each regressor.

In fMRI analysis, the convolved regressors are specified in the form of a design matrix (X $\beta$) (Fig.2.4), for any experimental design or nature of hypothesis testing, the design matrix defines further analysis steps. In the design matrix, each regressor corresponds to a column that are experimental conditions of interest. And the rows in the design matrix correspond to each data point. In fMRI, the scan images represent data points over time. Given the navigational behaviour, a GLM helps us relate the observed data to the one we expect to see, by expressing the observed neurophysiological responses (Y) as a linear combination of expected variables (X) and some residuals ($\varepsilon$).

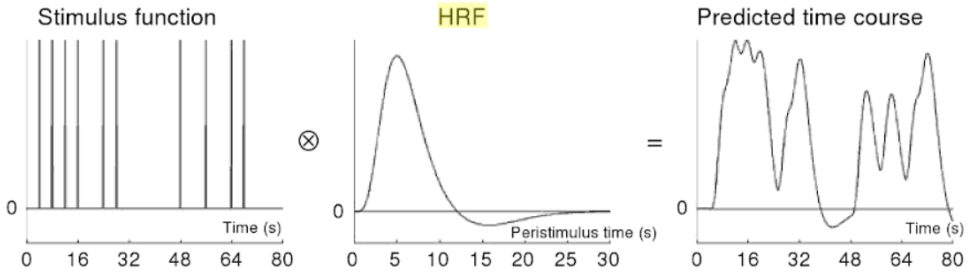


**Figure 2.2:** HRF convolution: The convolution of stimulus functions with a canonical hemodynamic response function to get the predicted time course for the stimulus. [Adapted from [14]]

The GLM analysis on fMRI data is done at voxel level. Consider a single voxel, which is a cube of a particular area within the 3D image. The voxel size and location remains the same throughout the experiment. The time series data of the BOLD activity within this voxel can be extracted from the multiple images acquired during the experiment. By running a GLM on this time series data we can get the beta value corresponding to the regressor for that particular voxel. If there are multiple regressor types, the analysis estimates the beta values for each regressor. Likewise, we run the GLM on the time series data of all the voxels separately. Eventually giving an image of results; voxel-wise beta values of whole brain for each regressor type.

### 2.2.3 Variables of interest: Regressors

The fMRI image data as such gives a lot of information about what happens within the brain during a task. Unlike most experiments where the regressors are designed before the experiment, here we retrospectively look at when the event of interest occurred during the experiment to extract the onsets time and their respective duration. The regressors of interest in this project are modelled using the navigation onsets. The onsets and their duration are extracted from a time series that have the real-time position and angular coordinates of the participants in the VR environment.

For HRF estimation, the regressors modelled rotation and locomotion onsets. The locomotion onsets were extracted from the changes observed in x and y coordinates of the participant in the VR. The time point that corresponded to respective change in any one of the coordinates from a stationary state gave a locomotion onset. The duration was defined as the time period between an onset and the subsequent stationary state. Similarly for rotation onsets, the point of angular change

resulted in an onset. As expected in a self-paced navigation task, the number of onsets were high. To compensate, the rotation onsets were divided into two independent: onsets- rotation right and rotation left. Thus, giving three independent regressor types in total. Further, all the onsets with duration less than 0.5sec were removed. Doing so, we removed all the erradic button tapping by the participant. Later these onsets and their durations were separated out into corresponding runs using the pulse time data that contained the time point for each TR [1].

### 2.2.4 Finite impulse response model

Finite impulse response model is considered to be the most flexible basic sets which make the least assumption about the shape of a BOLD response. FIR model is a set of basis functions delayed in time that model beta estimates for time points following a neural event. Instead of convolving the regressor with a canonical HRF model, here the estimates of a set of stick functions for specific time points to explain the BOLD response. Thus giving the actual shape of the response over the specified time window. The adequate number of stick functions and the length of time window should be chosen considering the data quality and TR.

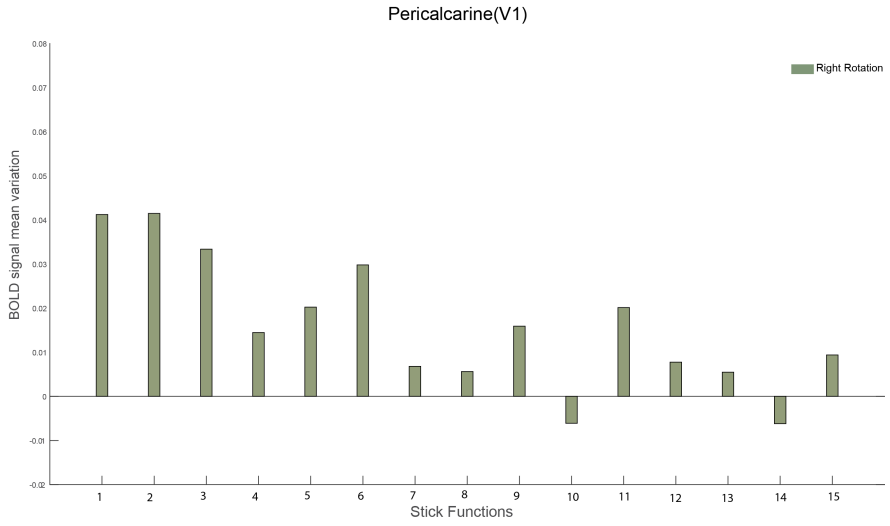


**Figure 2.3:** FIR- Stick functions: Finite impulse response model : Our FIR model has 15 stick functions evenly placed at fixed time points across the time window of 20 sec (a stick function every 1.33 sec). Each estimated stick function here represent the mean BOLD signal variation for right rotation onsets. The plot represent the HRF of pericalcarine sulcus from one participant.

[1] Repetition time- Time points that corresponds to image acquisition, in our case TR = 2.756 sec

In this study, we modelled the HRF using a FIR model across a time window of 20 seconds with 15 basis/stick functions. Each of the basis functions weight unit impulses that occur at time t =1.33, 2.66 to 19.99sec ; after an onset, modeling a weighted stick function every 1.33 second (20 sec/15 basis functions=1.33sec)(Fig.2.3). This value can be changed by varying the window length and number of stick functions. The t is different from a imaging TR. Here t refers to a sub-resolution time point where the model estimate a beta using the data acquired from the imaging TR's, which is nearest time point. Each of the 15 stick functions are regressors which model the activity of locomotion and rotation onset for the time window. For instance, in a single experimental run there are on average 100 locomotion onsets. Using the FIR model, the subsequent brain activity due to all of the locomotion onsets were weighted in 15 stick functions. The estimation of the betas is an ordinary least squares (OLS) solution and is carried out for all the voxels. The estimated betas represent the BOLD activity across the specified time window, which is the Hemodynamic response function (HRF) for the particular regressor.

Likewise, we estimated the betas from each stick function for all the three onset types. The voxel-wise beta values were mapped across the whole brain for each stick function, giving 15 functional maps of the brain. We created 45 maps (15 beta maps*3 onset types) per run for each participant. The respective betas for each stick function were averaged across runs to give the HRF for each voxel.

### 2.2.5 Design Matrix

While designing the design matrix, we had 15 stick functions as subset to each of the three onsets types. These regressors stayed as columns in the matrix that corresponded to the experimental variables of interest. As the rows in the design matrix represent the data points, we had the 4D fMRI images representing the rows (210- 3D images per run) (Fig.2.4). Alongside the main regressors, we added the six nuisance regressors which factored the motion correction parameters. Likewise, the design matrix was modelled for all runs per participant. These design matrices were used for previously mentioned beta estimation.

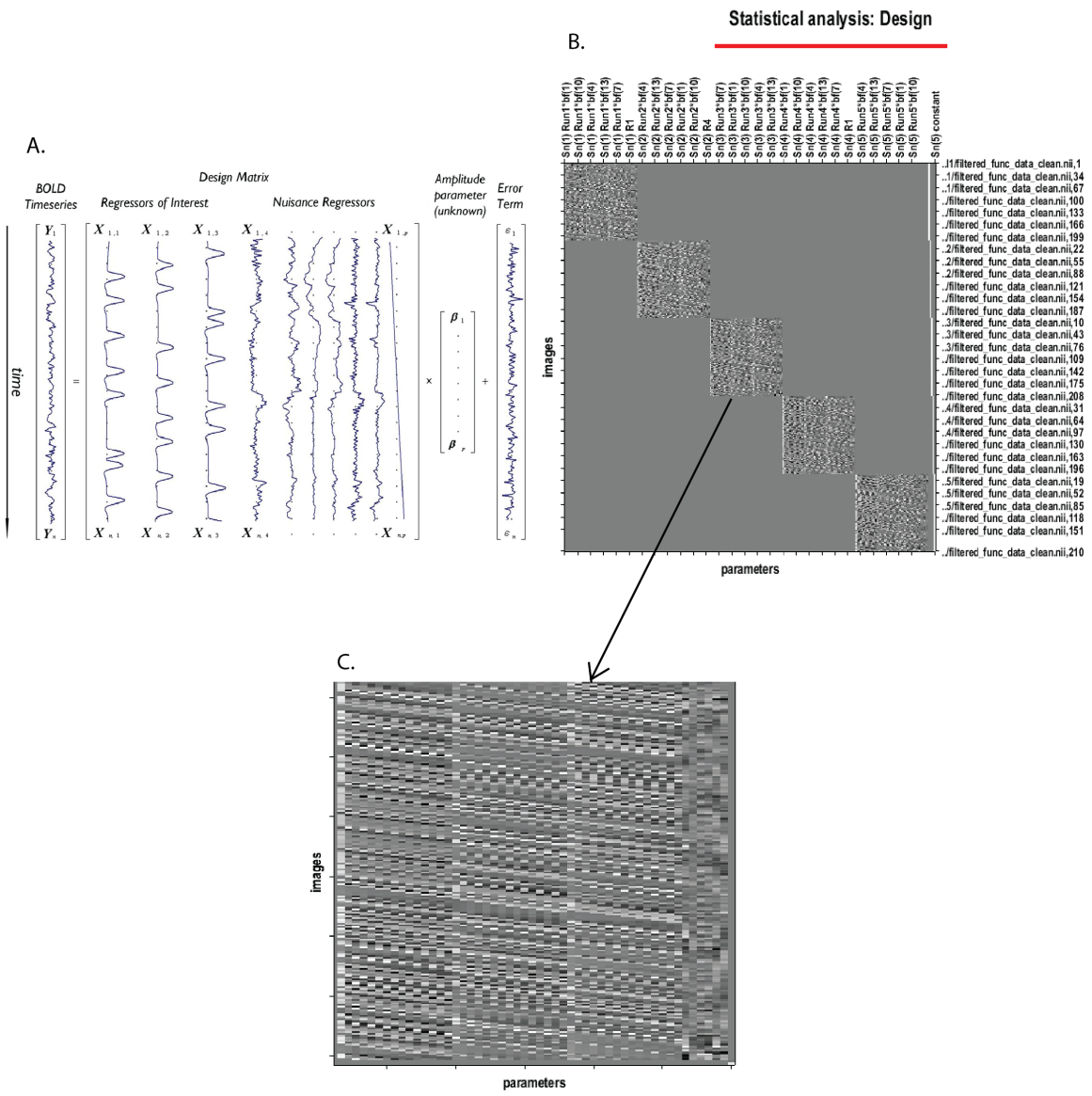


**Figure 2.4:** Design matrix: [Fig:A]. Representation of the General Linear Model (GLM) for a voxel with time-series Y predicted by a design matrix X. This example include three regressors of interest and nuisance regressors. Calculated betas( $\beta$) corresponding to each regressor are placed in amplitude vector ($\beta$). Vector '$\varepsilon$' contains calculated error terms to each time point ( adapted from [29] ). [Fig:B] The design matrix for one participant across 5 runs, *x* axis representing the regressors and *y* axis representing the data points(images). [Fig:C] Zoomed design matrix for one run, showing three 3 main blocks of regressors, each block containing 15 regressors representing 15 basis/stick functions of locomotion , left or right rotations. The right end of the image represents the six nuisance regressors for motion correction.

## 2.3 HRF-parameter extraction

Next, we extracted the HRF parameters from the regression output. Our extraction procedure builds on several individual steps. The extraction was carried out from the estimated HRF for every voxel. Firstly, we created HRF kernels from the canonical HRF model that vary in the delay to peak (sec) value. The parameters were extracted by curve fitting the estimated HRF with the HRF kernels. The amplitude and delay to peak values were extracted from the best fit. This procedure was carried out for all the voxels across all participants. The canonical HRF is the most commonly used model in fMRI analysis, below I briefly explain the characteristics of the model and later how it is used to build the kernels .

### 2.3.1 HRF kernels

#### Canonical HRF

The Canonical HRF (CHRF) is considered as the typical BOLD impulse response, it is modelled in the SPM toolbox [14] as a linear combination of two gamma functions(Fig. 2.5. In this model the only unknown or flexible parameter is the amplitude (A). The CHRF is characterised by a delay to peak ($\alpha 1$) of 6 seconds and undershoot delay ($\alpha 2$) of 16 seconds.The CHRF model do not have a initial dip. The CHRF is used to convolve the stimulus function to get task related regressor (Fig.2.2) which is used in the design matrix for GLM analysis. The model is popular due to its simplicity and robustness. For most event-related fMRI data analysis, the canonical HRF and its temporal and dispersion derivative seems to give a reliable detection of neural activity[30]. The model is inflexible considering only one unknown parameter (A) in the model.

$$h(t) = A\left(\frac{t^{\alpha_1-1}\beta_1^{\alpha_1}e^{-\beta_1 t}}{\Gamma(\alpha_1)} - c\frac{t^{\alpha_2-1}\beta_2^{\alpha_2}e^{-\beta_2 t}}{\Gamma(\alpha_2)}\right)$$

**Figure 2.5:** Canonical HRF Equation: where *t* refers time, $\alpha 1$= 6, $\alpha 2$= 16, $\beta 1$ = $\beta 2$ =1 and *1/6*, $\Gamma$represent the gamma function. The only unknown value is amplitude 'A'.

### HRF kernels

The above mention terms in the CHRF equation are dependent on each other. Changing one of the terms will give a different HRF shape. We created HRF kernels by varying the delay to peak (sec) value ($\alpha 1$) and setting the time window to 20 sec matching the time window of estimated HRF. Considering the possible variation in the true HRF shapes, we created kernels with all HRFs that peaked between 2 sec to 10 sec with 0.5 sec difference from one another. We had 17 HRF kernels with different attributes, which were used to fit the HRF estimated using FIR model.

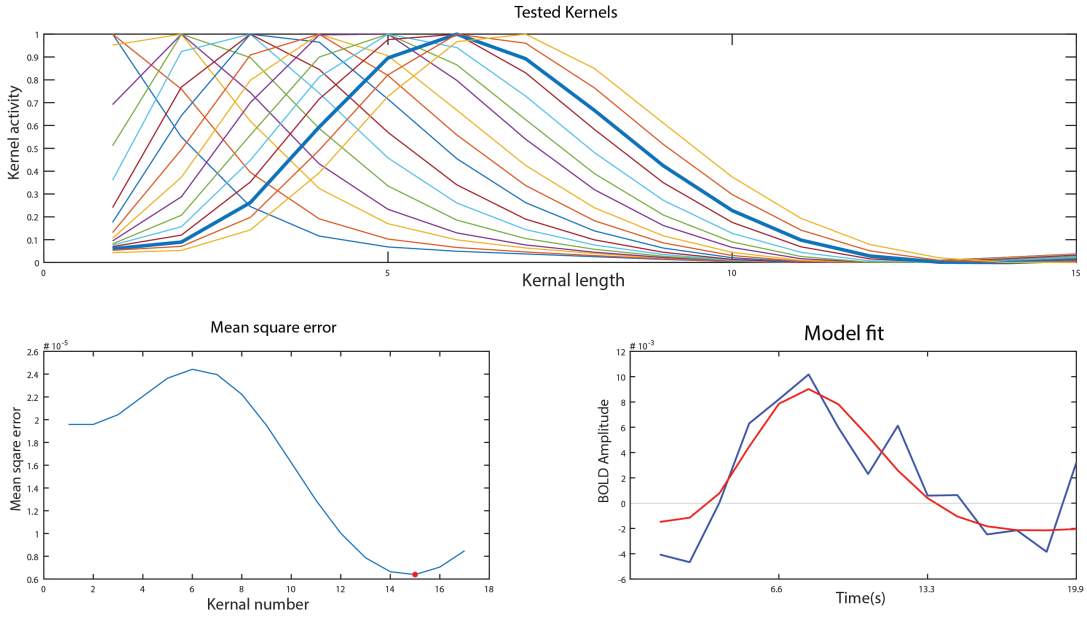


**Figure 2.6:** Parameter extraction: (1) 'Test kernels' : the HRFs with varying delay to peak latency, highlighting the best fit for the data (2) 'Mean square error': selection of the best fitting kernel(red star)to the data using the mse loss function (3) 'Model fit': The data (blue) and the selected kernel (red)

## 2.3.2 Curve fitting

The created kernels were iterated through the estimated model from every voxel to find the best fitting kernel for each voxel. The best fit was the HRF kernel that fits the data with least mean square error (mse).The Y-hat [2] values of the best fitted kernel were estimated and the highest value

[2]Y-hat represent the predicted values for a line that best fits in a linear regression. Here, for each time point we get a particular predicted value. We get 15 values that represent a line that best fits the data.

from the Y-hat matrix was taken as the amplitude value of the voxel. And the delay to peak for the selected kernel was extracted as the delay to peak of the voxel.(Fig.2.6). This extraction step was done on all participants for both the rotations and locomotion onsets.

## 2.4 Statistical inference

### 2.4.1 Voxel-wise analysis

The first level analysis gave us the HRF for all the voxel across all participants. The estimated HRFs were used to extract the amplitude and the delay to peak, which were mapped as separate whole brain images allowed us to visualize the variations in these parameters across brain regions corresponding to each onset type.

All the amplitude images across participants were smoothed separately for each onset in SPM using nearest neighbor interpolation method. The smoothed images were used for second level or group level analysis to find the regions that had threshold activity across all participants. To find the delay to peak (sec) in group level, the median across all the participants were calculated to create a brain image showing the median delay to peak (sec) across all regions during a specific navigational onset. We also mapped the mean squared error values corresponding to each voxel from the parameter extraction. The map from group analysis showed regions that had high and low mse values which indirectly represented the success of curve fitting procedure. The results of this analysis are shown in (Fig.3.6)

### 2.4.2 Regions of interest analysis

#### ROI definition

The region of interest (ROI) analysis refers to analysis on a selected cluster of voxels within the brain where the investigators interest lies. The region can be selected by creating a search space or by using anatomical atlases available in toolboxes like SPM, FSL or Freesurfer.

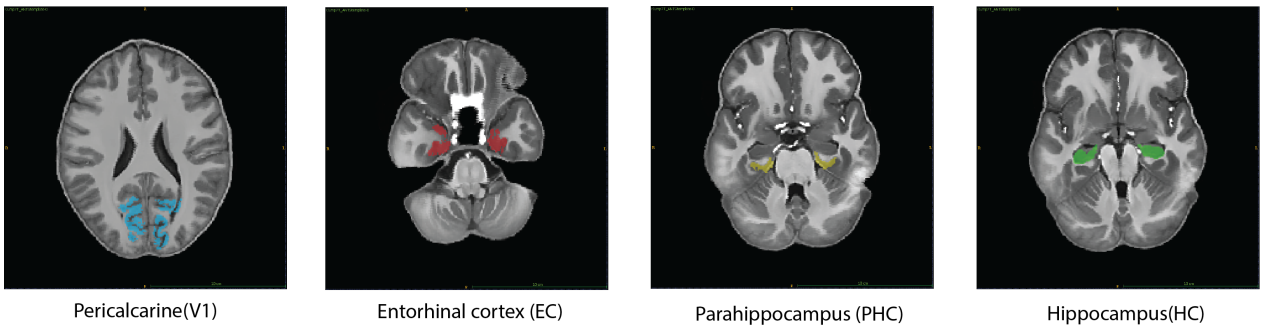


**Figure 2.7:** Freesurfer region of interests : Each of the ROI's and the analysis results from the respective ROI's were colour coded (V1- Blue, HC- Green, EC- Red, PHC- Yellow)

Here we used the Freesurfer atlases where neuroanatomical labels of each location were modelled based on probabilistic information from a great number of manually labeled training set that gave the geometric information and neuroanatomical boundaries of brain regions. The ROI's were extracted from the Freesurfer atlas. These binary ROI atlases were normalized and coregistered (aligning with functional images) with the common MNI [3]space (Fig.2.7). The ROI's we were interested in were the Pericalcarine(V1), Hippocampus(HC), Parahippocampus(PHC) and Enthorinal cortex(EC). These regions were chosen considering the activity shown and spatial coding characteristics mapped in these regions during previous navigation tasks. Each of the ROI's and the analysis results from the respective ROI's were colour coded (V1- Blue, HC- Green, EC- Red, PHC- Yellow)

### ROI-based inference

The ROI analyses were conducted using unsmoothed data. The selected ROI maps were used to extract the estimated basis functions (15 stick functions) for the voxels within the ROI region. The median across these HRFs within a ROI were calculated to give the ROI specific HRF. For all 18 participants, the HRFs corresponding to the ROI's were found for the rotations (left and right) and locomotion onsets. Thus, giving three estimated HRF for each ROI.

Further, to evaluate how the HRF parameters varied across participants and regions, the region

[3] MNI space(Montreal Neurological Institute space) space was developed by the Montreal neurologival institute to define a brain that could be used as a representative of the population. They used large series of MRI scans on normal controls to manually define various brain regions.

specific HRFs were used to extract the amplitude and delay to peak value by curve fitting to the HRF kernels created for voxel wise extraction. Considering that not all voxels within the selected ROI showed activation, to reduce the noise from non-active voxels, we extracted the top 50 percent of voxels that showed least mean squared error in the curve fitting (Fig.4.1, 4.2). The HRF and their parameters from the voxels were estimated across the participants. (Fig. 3.1, 3.4, 3.3, 3.5)

## 2.5 Comparison study

The previous steps in the study helped us evaluate the HRF and the parameters across participants and regions. To evaluate the estimated model efficiency compared to a commonly used canonical HRF model, we did a correlation study using these two models. Firstly, we split the data into training runs and test runs to avoid double dipping [31]. The convolution of both HRF with a boxcar function generated the corresponding predicted BOLD timeseries for test runs. The predicted time series were correlated with observed timeseries from test runs. For the correlation study was only carried out for locomotion onsets.

### 2.5.1 Training runs and Test runs

The experiment was divided into different runs during data acquisition. Most participants had 5 runs. The test runs were runs 2 and 4. The remaining of the runs were used as the training runs. The training runs were used to estimate the voxel wise HRF for the selected ROI's. The results from training run were used to correlate the data from test runs.

### 2.5.2 Convolution

#### With Canonical HRF

The widely used canonical HRF convolution was conducted on the test runs to estimate the predicted time series. A boxcar function of all the onsets of the test runs were modelled. The canonical HRF was down-sampled( seconds to milliseconds ) to the time resolution of boxcar function. Each onset from the boxcar function were then convolved with the canonical HRF to give a predicted BOLD time series. (Fig.2.8)

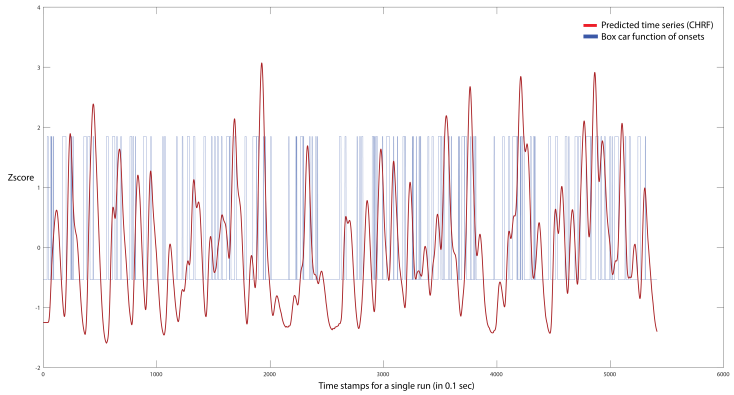


**Figure 2.8:** CHRF convolution: The blue line represent the boxcar function created using the onsets and their duration. The red graph shows the predicted time series modelled by convolving the canonical HRF with boxcar function.

#### With Estimated HRFs

As an alternate to convolving a CHRF , we used the optimal kernel associated with each individual voxel from the training runs to convolve with the boxcar function from the test runs. We did the similar down-sampling mentioned above to fit the time resolution of boxcar to get the predicted time series. By using the selected kernels, we created different predicted time series for each individual voxel. After convolution, these predicted time courses were again up-sampled to match the temporal resolution of the imaging data.

### 2.5.3 Predicted model and true BOLD response

We had two predicted models, one created with the CHRF and another from the best fit of FIR based HRF. Both the predicted BOLD time series were correlated to the actual BOLD time series data of test runs. Using Spearman-rank correlation to evaluate our model's efficiency for predicting the observed BOLD signal, we then compared to the CHRF model.(Fig.3.7)

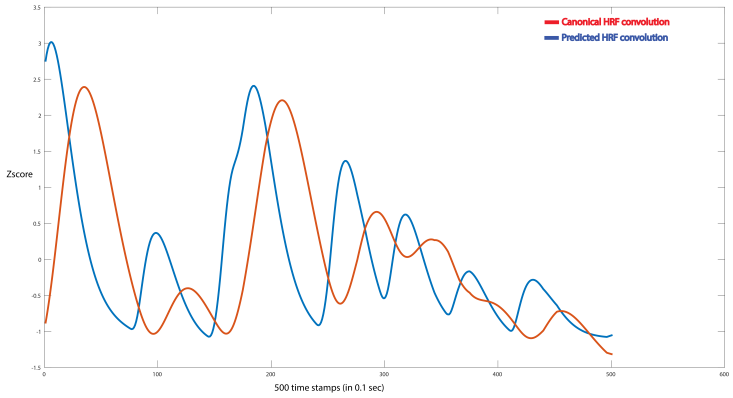


**Figure 2.9:** PHF and CHRF convolutions: The plot shows the canonical and estimated HRF convolutions for similar onsets. The delay to peak for the selected HRF kernel is lower than the canonical HRF, hence the visible shift in the time series.

Chapter 3

# Results

The objective of the thesis was to estimate the hemodynamic response function during a navigation based object-location memory task. This chapter we present the estimated HRF across the participants and selected regions. The section focuses on the results from two types of onsets: locomotion and rotation. We also plot the whole brain topology map which helped us visualise the delay to peak and amplitude values across different brain regions. The regions with threshold activity on group level was mapped, showing the regions activated during navigation and planning. In the ROI wise analysis, we determine the HRF of 4 main regions which have shown significant functional importance during previous navigation related studies[32]. The extracted HRF parameters across these regions were plotted, showing variation across participants and regions. The last section covers the comparison study between the predicted BOLD signal using the estimated HRF and canonical HRF.

## 3.1 Locomotion and rotation regressors

The locomotion and rotation onsets referred to the stimulus function that corresponded to the points when the subject started moving forward or rotated (changed their field of view) while trying to locate the objects in the virtual environment. The number of rotation onsets was higher than the locomotion onsets. The number of onset were reduced by removing all the onsets with duration less than 0.5 sec, thereby removing all the short instant button tapping by the participants during the experiment. Even after this step, an average of locomotion onsets stayed around 100 per run.

## 3.2 ROI analysis

The ROI wise analysis was carried out for 4 regions, which had significant importance during a navigational task. The median of all the HRF estimated from the voxels within each ROI (Fig.2.7) gave specific HRF shapes for each region. The median HRF was plotted across all participants, showing the variance in shape across participants and regions. The plots were colour coded consistently in all the results which corresponds to respective regions.

### 3.2.1 Locomotion HRFs

The HRFs for the locomotion onsets were plotted across (Fig.3.1) the 4 ROI's. The plot for Peri-calcarine (blue) showed the characteristics of the theorized HRF with an initial dip, a peak value

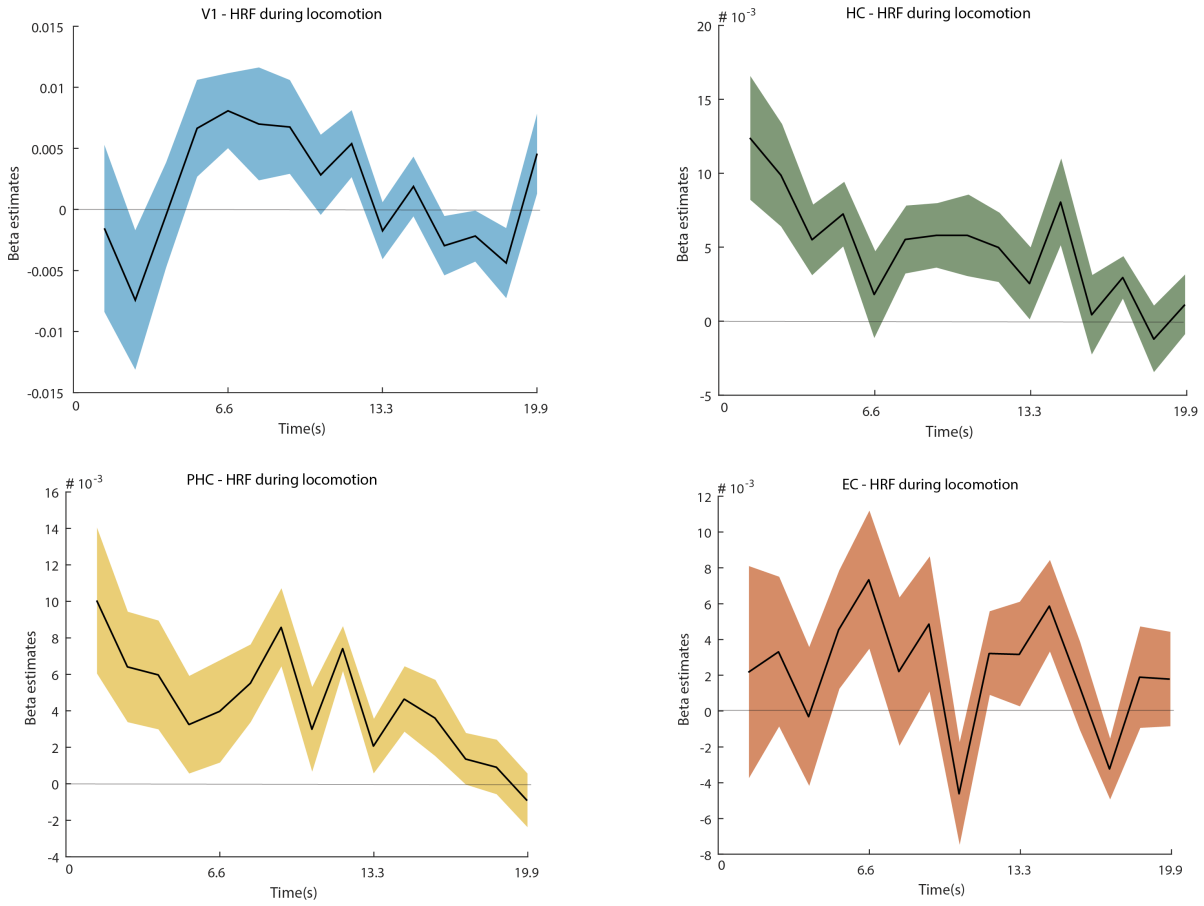


**Figure 3.1:** Hemodaynamic response function for locomotion onsets across the 4 ROIs: The black curve represent the mean HRF across 18 participants and the coloured regions represent their standard error of the mean(SEM).

and a post stimulus undershoot. The hippocampus (green) and parahippocampal (yellow) HRFs started with a peak and a gradual undershoot. The HRF in these two regions failed to estimate the initial dip and the steep ramp to peak. The entorhinal (red) HRF was noisy with visible fluctuations across time. The amplitude values in entorhinal cortex were lower compared to other regions. Nevertheless, we see an initial dip and a peak around 6 seconds.

### 3.2.2 Rotation HRFs

The HRFs for rotations were estimated as two separate onsets for left and right rotations. The estimated results for both type of rotations showed region wise similarity(Fig.3.2 . We combined both HRFs from the rotations and plotted their mean(Fig.3.3). Unlike the locomotion HRF for pericalcarine(blue), for rotations the HRF starts with a peak value, missing the initial dip and the steep to reach peak. The function drops eventually going below the base line. In case of hippocampus (green), parahippocampus (yellow) and entorhinal cortex (red) we see a clear HRF which was not seen in locomotion onsets. For all three regions we see a initial dip and a consistent amplitude above baseline. The HRF from entorhinal cortex shows similarity with its locomotion HRF counterpart, representing a sudden steep peak around 6 seconds in both cases.

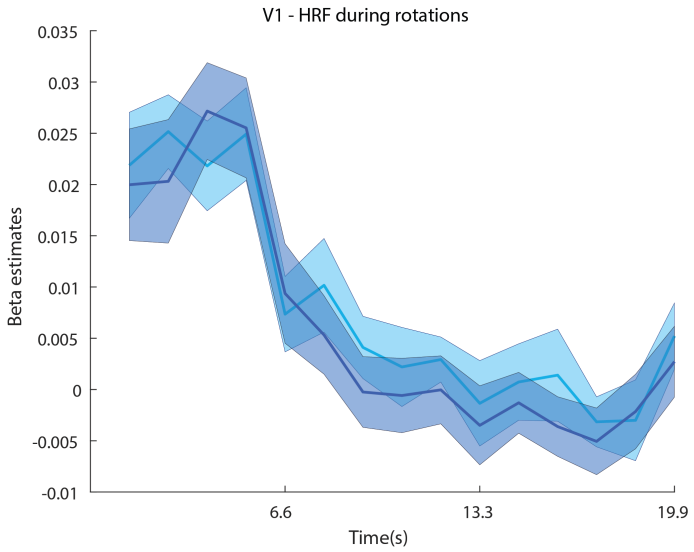


**Figure 3.2:** HRF-Visual cortex for Rotations: The two shades of blue represents left and right rotations. The curve correspond to the mean across participants and the coloured region depict the SEM. The left and right rotations elicited striking similar BOLD responses, as expected for visual regions

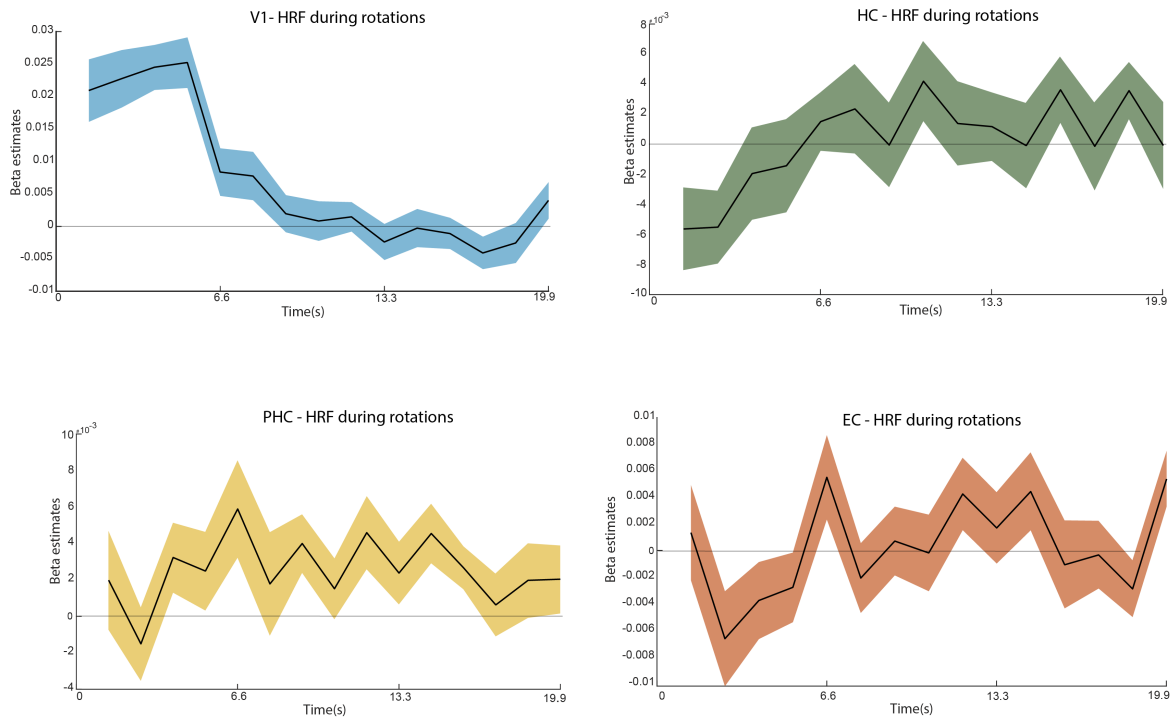


**Figure 3.3:** Hemodaynamic response function for rotation onsets across the 4 ROIs: The black curve represent the mean of rotation onsets (both left and right combined) across 18 participants and the coloured regions represent their standard error of the mean(SEM).

## 3.3 Amplitude and Delay to peak values

The amplitude and delay to peak values were estimated from the parameter extraction. The parameters were extracted from the median HRFs estimated across the ROI's. The bar plot shows the variation of the parameters across participants in their respective ROI's.

### 3.3.1 Parameters from locomotion onsets

For locomotion (Fig.3.4) , we see a consistent BOLD signal. Surprisingly the amplitude values are high for hippocampus (green) and parahippocampus (yellow), considering that they are subcortical regions. The error bar suggest significant variance in amplitude across 18 participants for all regions. The entorhinal cortex (red) has the highest fluctuation in ampliude, which is seen in the HRF shape mentioned in the previous section. The peak latency is highest for Pericalcarine sulcus (blue)

with a average value of 5.5 seconds, close to a canonical HRF peak (6 sec). The lowest latency to peak is seen in hippocampus (green).

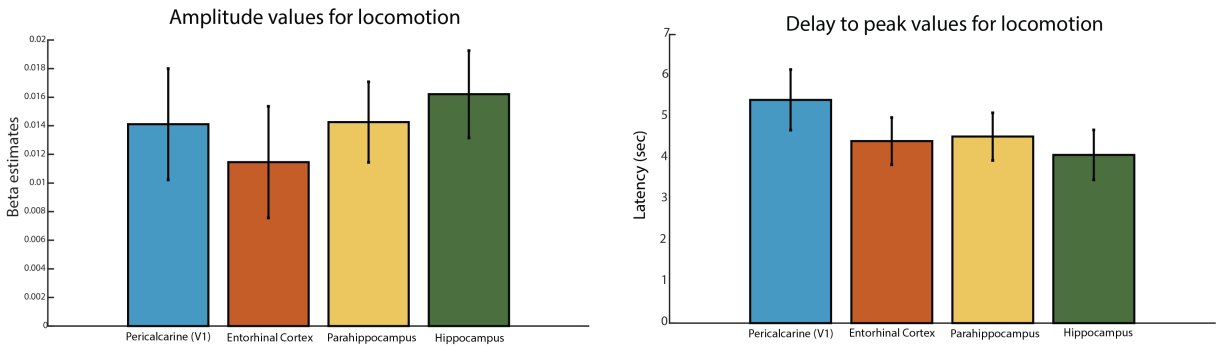


**Figure 3.4:** Locomotion Parameters: The mean of extracted parameters across participants for locomotion onsets represented for different regions. Error bar showing the SEM across subjects.

### 3.3.2 Parameters for rotation onsets

For rotation (Fig.3.5), we see a massive difference in amplitude between the Pericalcarine sulcus(blue) and other regions. All the three subcortical ROI's show low amplitudes. The variation in amplitude is lower for rotations compared to locomotion across participants. The delay to peak values are highest for hippocampus( green ) and parahippocampus (yellow), with values around 5.5 seconds.

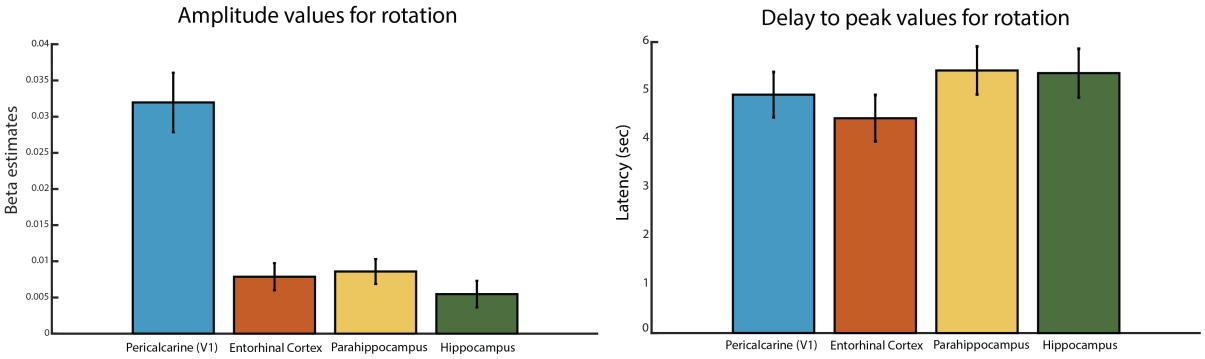


**Figure 3.5:** Rotation Parameters: The mean of extracted parameters across participants for rotation onsets. Error bar showing the SEM across participants

## 3.4 Whole brain maps

The brain maps were created by assigning the estimated parameters to each voxel location. Second level analysis using the smoothed amplitude maps across the participants gave regions with threshold amplitude values. The result showed higher amplitudes in expected regions like V1 and prefrontal cortex. There were activation in some voxels in subcortical structures like hippocampus, entorhinal cortex and parahippocampus.

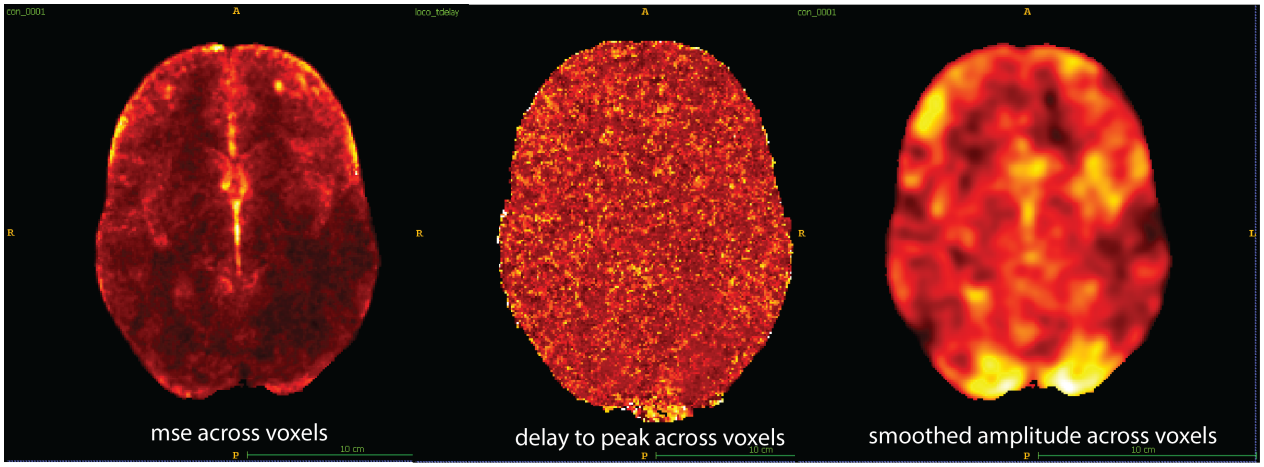


**Figure 3.6:** Whole brain maps: The three maps shown are from the second level analysis of extracted parameters. The bright colour represent higher values. Amplitude map shows high activity in visual cortex and prefrontal cortex. The delay to peak map shows clusters of regions with similar value. The dark regions in mse map depict the regions that had least mean squared error while curve fitting.

The median map of the delay to peak(sec) values across participants show clusters of voxels in different brain regions with consistent values. The result indirectly represent the regions activated. The regions showing higher amplitude values have consistent delay to peak values. The peak latency varied across regions, which could infer in variation across different regions. The regions with higher mse values showed regions that did not fit well during curve fitting. The regions like visual cortex showed low mse values suggesting the success in finding a best fit during curve fitting,

## 3.5 Predictive modeling

The Spearman correlation between the observed BOLD time series and the predicted time series showed comparable results for estimated and canonical HRF. For the HRF estimated for locomo-

tion onsets, the correlation is slightly higher than the CHRF in visual cortex (blue). The other regions had very low spearman rho values for both HRFs. Surprisingly, the hippocampus region had negative correlation with both predicted time course.

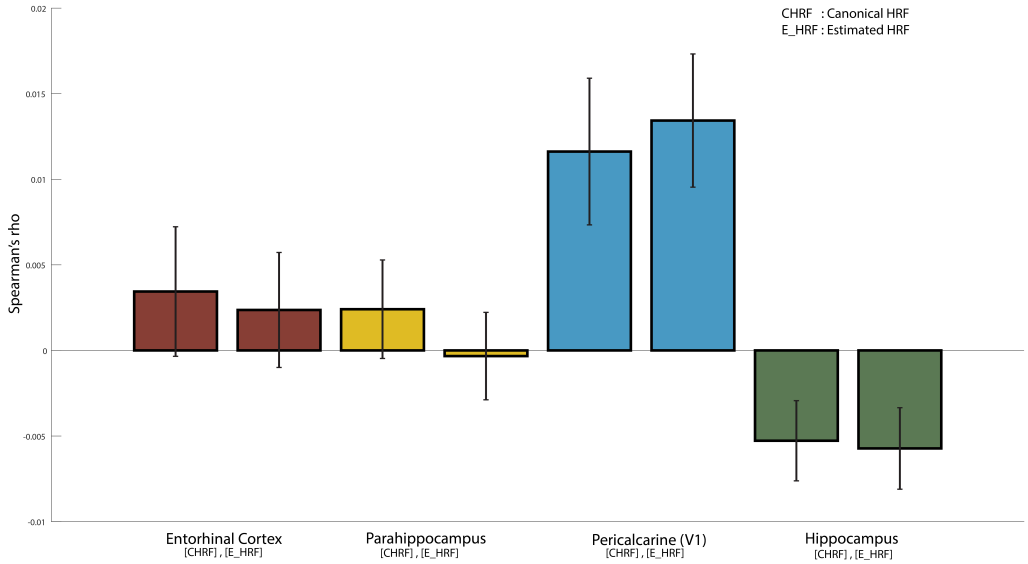


**Figure 3.7:** For locomotion onsets, the Spearman correlation between predicted time course using both the HRFs and test runs data.The graph representing the correlations in 4 different regions. The first bar of each colour represent the canonical HRF correlation(CHRF) and the neigbouring one represent the estimated HRF correlation(EHRF) V1 showing higher correlation for estimated HRF when compared to canonical HRF. Hippocampal region represent a negative correlation with both the predicted time series.

Chapter 4

# Discussion

## 4.1 Overview

In this study, we estimated the HRF during a self-paced navigation task using a finite impulse response model. The modeling was carried out for events related to participants navigating in a VR paradigm. Unlike most navigation based studies where they estimated a beta for the whole time period, here we model basis functions for each time point following an onset. This helped us understand the characteristic variation in HRF across different regions. We estimated the HRF for brain regions involved in visual perception and navigation. The estimated HRF shapes across different regions resemble a theorized HRF, with a initial dip, a peak and a post stimulus undershoot. The extraction of HRF parameters showed their variance across regions and participants. The study stands out by demonstrating the diversity in HRF shape during a navigational task. Our study provide evidence to support the concerns of how the variation in HRF could lead to mis-specifications in fMRI data analysis. We also validated the model efficiency by comparing the predicted BOLD signal modelled using our estimated HRF and the canonical HRF.

## 4.2 The human navigation network

The human navigation network studied here mainly focuses on four different brain regions. A navigation task activates these regions, which are studied broadly to understand the navigation cognition in humans[33][32].

Our task relies on visual cues that helped participants navigate in the VR environment to find the object location. Studies have shown how navigation is strongly driven by vision, which modulates the activities in different cortical regions.[34][35][36][37]. The estimated HRF for the pericalcarine (visual cortex) during locomotion (Fig.3.1) clearly depicts a HRF character, this shape is seen in numerous studies, which initially lead to the modeling of the canonical HRF for fMRI studies[14]. The region showed the highest activity among other modeled regions. Here the HRF peaks around 6 seconds, matching the CHRF model[14]. The rotation onsets for the same region produced a peak at the point of onset(Fig.3.3). The earlier peak during rotation could be due to the eye movement that precedes the button presses[38]. The button presses that correspond to rotation caused bigger changes in visual cues resulting in a greater optic flow compared to locomotion related button presses. The higher amplitude during rotation could be due to this higher optic flow. The consequence of optic flow[39]during navigation and spatial attention[40]is an established study in other primates. The higher amplitude in the visual cortex compared to other regions could also be due to MR coils, which are closer to this region than other deeper brain regions studied here. The results of estimated HRFs for pericalcarine validates the estimation and extraction procedures used in this study due to the characteristic similarities seen from previous studies[41].

Hippocampal activity is well documented in VR studies when participants used a cognitive map based strategy to create shortcuts or plan novel routes during a navigation task[32]. The estimated HRF in the hippocampus during locomotion onset (Fig.3.1) showed a negative response. The peak at the beginning of the estimated HRF could presumably be an activity related to the decision making process in the hippocampus that occurred seconds before the actual onset. Supporting this inference, in a self-paced VR experiment, the movement initiation periods have shown higher activity in the hippocampus[42]. Studies have predicted hippocampal representation of the future locations during a goal-directed behavior, reflecting the importance of the region for navigation[43]. A similar HRF shape is see in our study for the parahippocampal region, which is often studied in parallel with the hippocampus for spatial representation. Unlike locomotion onsets, for rotation we see the normal characteristics of the HRF in both regions. This could suggest a difference in how the regions respond to locomotion and rotation.

The Entorhinal cortex is considered as one of the central regions alongside the hippocampus

where we find functionally defined cells[44], which is studied in humans for understanding the coding principles that result in spatial representation[33]. Our estimation from the entorhinal cortex characterised a peak around 6 seconds both for locomotion and rotation. The HRF model looked noisy with visible fluctuations. The functional images from our data cuts out a large portion of voxels from the entorhinal cortex during data acquisition, this could be a reason for the low amplitude values resulting in noisy data.

The parameter extraction gave the amplitude and delay to peak values across regions and participants. The mean of these parameters across participants showed consistency. For locomotion onsets (Fig.3.4), the delay to peak varies from 4.5sec to 5.5 sec across the regions. The amplitude values for locomotion was highest in the hippocampus, suggesting the functional importance of the region during locomotion. For rotation onsets (Fig.3.5, the delay to peak varies from 4.5 sec to 5.5 sec across regions. The amplitude value for rotation was highest for visual cortex, showing drastic difference compared to other regions.

## 4.3 Variation in HRF

There is a continuing challenge of understanding HRF variation in fMRI study. Even though we see variation in the HRF across regions, these effects were small and did not survive the statistical testing. The shape of the estimated HRF across different regions showed the characteristics of a theorized HRF[14]. The initial peak in some regions mentioned above could be due to inaccuracy in modelling the correct onset. The speculations mentioned could suggest that the HRF we modeled for some regions missed the initial HRF characteristics, which might have occurred before the modeled onset (button presses). These inter-stimulus events that led to the button presses are not modeled. The estimated model only had the HR starting from the button presses. Most studies use the button presses as the onset to do various statistical testing. Studies have shown that a 1 sec misestimate of the delay to peak could affect the magnitude fit by 10 percent and a 2 sec misestimate would lead to decrease in magnitude by 38 percent[23]. In our object-location memory task, the regions we study for spatial representation could involve these initial cognitive processes that led to the events( button press). This misestimation could lead to drastic differences between the observed and predicted BOLD signal. In the correlation study we conducted for hippocampus,

both the predicted time series showed negative correlation to the observed BOLD response. This could mean that none of the models work well in some regions or these regions have a totally different HRF character. A recent study that supported this claim have shown negative HRF maps in visual cortex, showing a entire network, which respond with characteristics opposite to currently theorized HRF [45] .

Other than the misspecifications caused during different HRF modeling and physiological factors, there are various other factors, which could influence the HRF. HR varies in its shape as a function of both the task and brain regions. Early studies from Aguirre [16] and Buckner[46] have shown these variations across participants and regions. The delay to peak values varied between 4-8 sec in gray matter and 8-14 sec in regions with large blood vessels, suggesting a longer time for blood to reach large vessels[47]. The vessel diameters and density within each voxel vary across brain regions and this is one of the major non-neural reasons for HR variation. In our study we don't see such large variations in delay to peak values across regions probably due to the inaccuracy in finding the best fit during parameter extraction. The high amplitude values in visual cortex and the similarity in low amplitudes in the other three closely connected subcortical regions could suggest the vasculature differences which led to HRF variations. Using a fixed HRF model will lead to misspecification in most brain regions [48]. The most common approach for these variabilities while doing a GLM analysis is to use multiple basis functions for each variables of interest. We decided to use FIR model considering the flexibility it offered to model a true HRF. Studies from Lindquist [49] have shown that FIR model do not show large biases and could account for large model misspecification and variation in timing and duration of onsets.

## 4.4 Which one is better?

The comparison study for locomotion onsets shows that the canonical HRF seems to be a good compromise between robustness and flexibility for our data. The estimated HRFs have better correlation in visual cortex, which showed the highest activity among the ROI's. The result suggest that the FIR model will likely outperform canonical HRF if provided with better data quality and accuracy in extraction of parameters, which was validated in visual cortex that had the highest number of active voxels.

## 4.5 Limitations and recommendations

Finite impulse response model is a great tool to model a HRF without giving any bias to a specific shape. Each basis set in the FIR allows you to have one free parameter for each time point within the time window, making it one of the most flexible model to estimate true HRF. FIR helped us study the variability of HRF across different regions for different conditions. The flexibility of FIR have advantages and disadvantages while modeling a HRF. For FIR model, without a high quality data the estimates will be noisy. The number of basis set determine the degree of freedom of the model, the increase in basis functions decrease the statistical power. In our study we used 15 basis functions, this number was selected to compromise between the resolution and robustness of the data. Our data had a TR of 2.756, which resulted in very few data points for the amount of onsets we had. The high TR and resultant data quality restricted our basis functions to 15. In addition, we modeled the 20 second time window considering the characteristics of a HRF, which reach a post stimulus undershoot around 16 second. The estimation can be improved by using a data acquired in shorter TR's, this will let us have more data points within the time window. Also, allow us to increase the number of basis sets, leading to more precise estimation of the shape of the HRF.

For the parameter extraction, we used the HRF kernels adapted from a canonical HRF by varying the delay to peak values. The parameters extracted do not show significant variation. The results could mean that the curve fitting using the different HRF kernels did not match accurately (Fig.4.5). We used the median HRF across all voxels within an ROI to extract the parameters, this could include a large number of voxels that do not show significant BOLD response. The curve fitting for these voxels would lead to false results, affecting the median values for a ROI. Estimating the HRF from top 50 percent of voxels that showed least mse during curve fitting have improved the shape and characteristics of HRF (Fig.(4.1),(4.2)). We chose MSE as a loss function for the extraction. However, there are other loss functions we could have used and this could potentially lead to more accurate HRF parameters. Future studies could test other loss functions directly against each other. Also, to validate the possible shift in the actual neural response related to movement initiation, we could study the data points before the button presses. This would likely give the true HRF characteristics in those mentioned regions.

The variation in HRF across regions and subjects is evident. To overcome this limitation in the future studies, we could acquire data solely for estimating the HRF for a particular task. Studies have shown that the estimated HRF from one participant was able to explain 72 percent of the variation in other participants[46]. Another alternative is do multiple scans on a participant and using a part of the data acquired to estimate a HRF. The HRF estimated from a ROI in the same subject in multiple scans varied much less than HRFs estimated from the same ROI across subjects[16]. Given with sufficient quality data, using a FIR model will produce better results.

## 4.6 Conclusion

The field of fMRI has developed rapidly over the years with better scanners and pulse sequences that improved the quality of acquired data. These developments improved our understanding of the brain immensely. However, much of what we know about human brain function is derived from studying hemodynamic responses following neuronal activity instead of studying this activity directly. A critical remaining challenge is to interpret these hemodynamic responses, a task for which, characterising these responses is imperative. The inter-subject and inter region differences in the responses are rarely acknowledged in fMRI studies. Our FIR model showed its flexibility in capturing the range of HR variations across different regions. The results could be improved if provided with more data and better extraction methods. We have shown that the canonical HRF seems to be a good compromise between the robustness and flexibility for our data, but also that the FIR model has the potential to perform better.

Here, we have shown that the HRF varies across regions and participants during a navigation task. Characterising the HRF variations in more detail will ultimately help us to avoid misspecifications that could occur while using a fixed HRF model and to improve our understanding of the brain in general.

# Bibliography


[1] Edward C. Tolman. Cognitive maps in rats and men. *Psychological Review*, 55(4):189–208, 1948.

[2] John O'Keefe and Lynn Nadel. Prcis of o'keefe amp; nadel's the hippocampus as a cognitive map. *Behavioral and Brain Sciences*, 2(4):487494, 1979.

[3] Edvard I. Moser, Emilio Kropff, and May-Britt Moser. Place cells, grid cells, and the brain's spatial representation system. *Annual Review of Neuroscience*, 31(1):69–89, 2008. PMID: 18284371.

[4] Jeffrey S. Taube. Head direction cells and the neurophysiological basis for a sense of direction. *Progress in Neurobiology*, 55(3):225 – 256, 1998.

[5] Colin Lever, Stephen Burton, Ali Jeewajee, John O'Keefe, and Neil Burgess. Boundary vector cells in the subiculum of the hippocampal formation. *Journal of Neuroscience*, 29(31):9771–9777, 2009.

[6] Hugo J. Spiers and Eleanor A. Maguire. A navigational guidance system in the human brain. *Hippocampus*, 17(8):618–626, 2007.

[7] Joshua Jacobs, Christoph T. Weidemann, Jonathan F. Miller, Alec Solway, John F. Burke, Xue-Xin Wei, Nanthia Suthana, Michael R. Sperling, Ashwini D. Sharan, Itzhak Fried, and Michael J. Kahana. Direct recordings of grid-like neuronal activity in human spatial navigation. *Nature Neuroscience*, 16:1188 EP –, Aug 2013.

[8] Matthias Nau, Tobias Navarro Schröder, Jacob L. S. Bellmund, and Christian F. Doeller. Hexadirectional coding of visual space in human entorhinal cortex. *Nature Neuroscience*, 21(2):188–190, 2018.

[9] Christoph Leithner and Georg Royl. The oxygen paradox of neurovascular coupling. *Journal of Cerebral Blood Flow & Metabolism*, 34(1):19–29, 2014. PMID: 24149931.

[10] Seiji Ogawa and Tso-Ming Lee. Magnetic resonance imaging of blood vessels at high fields: In vivo and in vitro measurements and image simulation. *Magnetic Resonance in Medicine*, 16(1):9–18, 1990.

[11] Nikos K. Logothetis. What we can do and what we cannot do with fmri. *Nature*, 453:869 EP –, Jun 2008. Review Article.

[12] MRI Questions. Hrf shape, 2019.

[13] Peter C.M. van Zijl, Jun Hua, and Hanzhang Lu. The bold post-stimulus undershoot, one of the most debated issues in fmri. *NeuroImage*, 62(2):1092 – 1102, 2012. 20 YEARS OF fMRI.

[14] K. J. Friston, A. P. Holmes, K. J. Worsley, J.-P. Poline, C. D. Frith, and R. S. J. Frackowiak. Statistical parametric maps in functional imaging: A general linear approach. *Human Brain Mapping*, 2(4):189–210.

[15] Geoffrey M. Boynton, Stephen A. Engel, Gary H. Glover, and David J. Heeger. Linear systems analysis of functional magnetic resonance imaging in human v1. *Journal of Neuroscience*, 16(13):4207–4221, 1996.

[16] G.K. Aguirre, E. Zarahn, and M. D'Esposito. The variability of human, bold hemodynamic responses. *NeuroImage*, 8(4):360 – 369, 1998.

[17] F.M. Miezin, L. Maccotta, J.M. Ollinger, S.E. Petersen, and R.L. Buckner. Characterizing the hemodynamic response: Effects of presentation rate, sampling procedure, and the possibility of ordering brain activity based on relative timing. *NeuroImage*, 11(6):735 – 759, 2000.

[18] Richard B Buxton. *Introduction to functional magnetic resonance imaging: principles and techniques*. Cambridge university press, 2009.

[19] Jonathan M Levin, Marjorie H Ross, Jack H Mendelson, Marc J Kaufman, Nicholas Lange, Luis C Maas, Nancy K Mello, Bruce M Cohen, and Perry F Renshaw. Reduction in bold fmri response to primary visual stimulation following alcohol ingestion. *Psychiatry Research: Neuroimaging*, 82(3):135 – 146, 1998.

[20] Jonathan M Levin, Blaise deB Frederick, Marjorie H Ross, Jonathan F Fox, Heidi L von Rosenberg, Marc J Kaufman, Nicholas Lange, Jack H Mendelson, Bruce M Cohen, and Perry F Renshaw. Influence of baseline hematocrit and hemodilution on bold fmri activation. *Magnetic Resonance Imaging*, 19(8):1055 – 1062, 2001.

[21] Michael D Noseworthy, Jeff Alfonsi, and Sonya Bells. Attenuation of brain bold response following lipid ingestion. *Human Brain Mapping*, 20(2):116–121, 2003.

[22] Daniel A. Handwerker, John M. Ollinger, and Mark D'Esposito. Variation of bold hemodynamic responses across subjects and brain regions and their effects on statistical analyses. *NeuroImage*, 21(4):1639 – 1651, 2004.

[23] Daniel A. Handwerker, Javier Gonzalez-Castillo, Mark D'Esposito, and Peter A. Bandettini. The continuing challenge of understanding and modeling hemodynamic variation in fmri. *NeuroImage*, 62(2):1017 – 1023, 2012. 20 YEARS OF fMRI.

[24] Tobias Navarro Schröder, Koen V Haak, Nestor I Zaragoza Jimenez, Christian F Beckmann, and Christian F Doeller. Functional topography of the human entorhinal cortex. *eLife*, 4:e06738, jun 2015.

[25] Jonathan D. Power, Anish Mitra, Timothy O. Laumann, Abraham Z. Snyder, Bradley L. Schlaggar, and Steven E. Petersen. Methods to detect, characterize, and remove motion artifact in resting state fmri. *NeuroImage*, 84:320–341, Jan 2014. 23994314[pmid].

[26] B.A. Poser, P.J. Koopmans, T. Witzel, L.L. Wald, and M. Barth. Three dimensional echo-planar imaging at 7 tesla. *NeuroImage*, 51(1):261 – 266, 2010.

[27] Christian F. Doeller, Caswell Barry, and Neil Burgess. Evidence for grid cells in a human memory network. *Nature*, 463(7281):657–661, Feb 2010. 20090680[pmid].

[28] Matthias Nau. fmri-preprocessing slides, 2019.

[29] Martin Monti. Statistical analysis of fmri time-series: A critical review of the glm approach. *Frontiers in Human Neuroscience*, 5:28, 2011.

[30] Richard N. A. Henson, Michael Hornberger, and Michael D. Rugg. Further dissociating the processes involved in recognition memory: An fmri study. *Journal of Cognitive Neuroscience*, 17(7):1058–1073, 2005.

[31] Nikolaus Kriegeskorte, W. Kyle Simmons, Patrick S. F. Bellgowan, and Chris I. Baker. Circular analysis in systems neuroscience: the dangers of double dipping. *Nature neuroscience*, 12(5):535–540, May 2009. 19396166[pmid].

[32] Russell A. Epstein, Eva Zita Patai, Joshua B. Julian, and Hugo J. Spiers. The cognitive map in humans: spatial navigation and beyond. *Nature Neuroscience*, 20:1504 EP –, Oct 2017. Review Article.

[33] Jacob L. S. Bellmund, Peter Gärdenfors, Edvard I. Moser, and Christian F. Doeller. Navigating cognition: Spatial codes for human thinking. *Science*, 362(6415), 2018.

[34] Daniel Christopher Haggerty and Daoyun Ji. Activities of visual cortical and hippocampal neurons co-fluctuate in freely moving rats during spatial behavior. *eLife*, 4, September 2015.

[35] Guifen Chen, John A King, Neil Burgess, and John O'Keefe. How vision and movement combine in the hippocampal place code. *Proceedings of the National Academy of Sciences of the United States of America*, 110(1):378383, January 2013.

[36] Aman B Saleem, E Mika Diamanti, Julien Fournier, Kenneth D Harris, and Matteo Carandini. Coherent encoding of subjective spatial position in visual cortex and hippocampus. *Nature*, 562(7725):124127, October 2018.

[37] Cristopher M. Niell and Michael P. Stryker. Modulation of visual responses by behavioral state in mouse visual cortex. *Neuron*, 65(4):472–479, Feb 2010. 20188652[pmid].

[38] Laura Piccardi, Maria De Luca, Raffaella Nori, Liana Palermo, Fabiana Iachini, and Cecilia Guariglia. Navigational style influences eye movement pattern during exploration and learning of an environmental map. *Frontiers in Behavioral Neuroscience*, 10:140, 2016.

[39] Aman B. Saleem, Asli Ayaz, Kathryn J. Jeffery, Kenneth D. Harris, and Matteo Carandini. Integration of visual motion and locomotion in mouse visual cortex. *Nature neuroscience*, 16(12):1864–1869, Dec 2013. 24185423[pmid].

[40] Carrie J. McAdams and R. Clay Reid. Attention modulates the responses of simple cells in monkey primary visual cortex. *Journal of Neuroscience*, 25(47):11023–11033, 2005.

[41] Serena K. Thompson, Stephen A. Engel, and Cheryl A. Olman. Larger neural responses produce bold signals that begin earlier in time. *Frontiers in Neuroscience*, 8:159, 2014.

[42] Raphael Kaplan, Christian F. Doeller, Gareth R. Barnes, Vladimir Litvak, Emrah Dzel, Peter A. Bandettini, and Neil Burgess. Movement-related theta rhythm in humans: Coordinating self-directed hippocampal learning. *PLOS Biology*, 10(2):1–13, 02 2012.

[43] Thackery I. Brown, Valerie A. Carr, Karen F. LaRocque, Serra E. Favila, Alan M. Gordon, Ben Bowles, Jeremy N. Bailenson, and Anthony D. Wagner. Prospective representation of navigational goals in the human hippocampus. *Science*, 352(6291):1323–1326, 2016.

[44] Edvard I. Moser, May-Britt Moser, and Bruce L. McNaughton. Spatial representation in the hippocampal formation: a history. *Nature Neuroscience*, 20:1448 EP –, Oct 2017.

[45] Tomas Knapen, Daan van Es, and Martijn Barendregt. Mapping the dark side: Visual selectivity of default network deactivations. *bioRxiv*, 2018.

[46] Randy L. Buckner, Wilma Koutstaal, Daniel L. Schacter, Anders M. Dale, Michael Rotte, and Bruce R. Rosen. Functionalanatomic study of episodic retrieval: Ii. selective averaging of event-related fmri trials to test the retrieval success hypothesis. *NeuroImage*, 7(3):163 – 175, 1998.

[47] Adrian T. Lee, Gary H. Glover, and Craig H. Meyer. Discrimination of large venous vessels in time-course spiral blood-oxygen-level-dependent magnetic-resonance functional neuroimaging. *Magnetic Resonance in Medicine*, 33(6):745–754, 1995.

[48] Rasmus M. Birn, Ziad S. Saad, and Peter A. Bandettini. Spatial heterogeneity of the nonlinear dynamics in the fmri bold response. *NeuroImage*, 14(4):817 – 826, 2001.

[49] Martin A. Lindquist, Ji Meng Loh, Lauren Y. Atlas, and Tor D. Wager. Modeling the hemodynamic response function in fmri: efficiency, bias and mis-modeling. *NeuroImage*, 45(1 Suppl):S187–S198, Mar 2009. 19084070[pmid].

# Appendix

### Least mean squared error voxels

During the curve fitting procedure, the HRF kernal that fits the best was estimated by finding the least mean square error with the actual data. The lower the mean square error , better the fit. Alongside the amplitude and delay to map maps created during voxel wise extraction, we also created the mse values corresponding to the each voxel. Later, to find the top 50 percent voxels that have the best fit was extracted by finding the top 50 percent of the voxels that had lower mse values. This gave us the top performing voxels. The HRF's estimated from these voxels across regions are plotted below fig.4.1, fig.4.2.

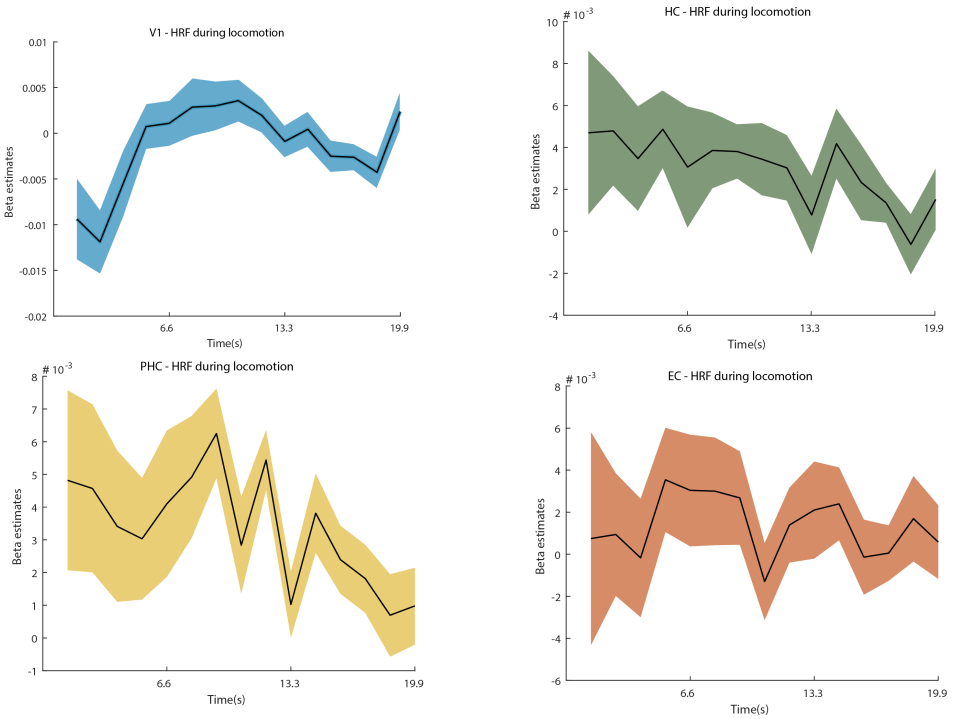


**Figure 4.1:** Locomotion HRF from top 50 percent of voxels with least mse during curve fitting

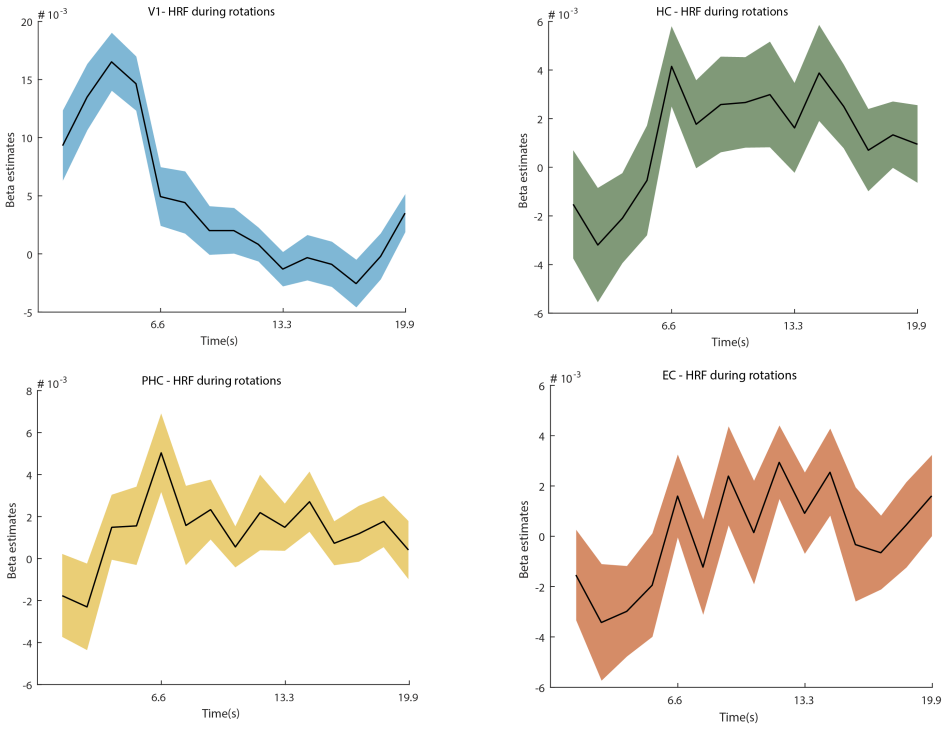


**Figure 4.2:** Rotations HRF from top 50 percent of voxels with least mse during curve fitting

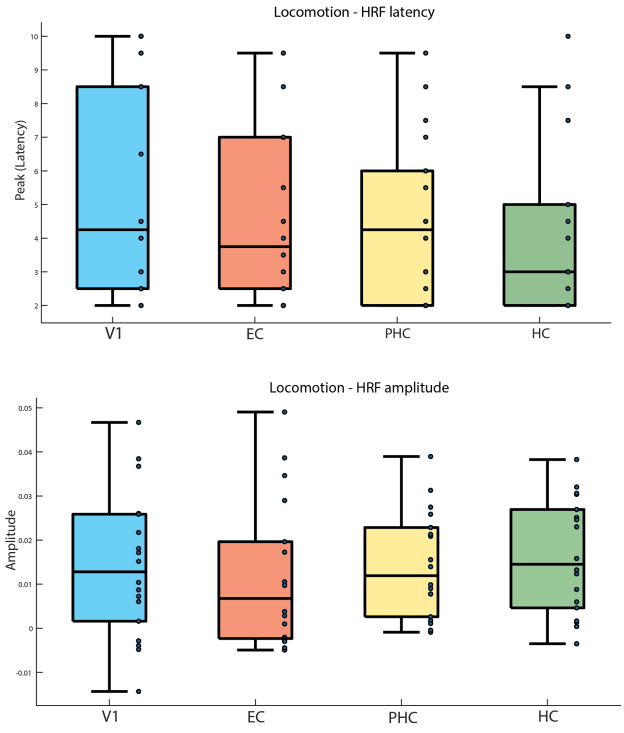


**Figure 4.3:** Locomotion parameters- median values

### Median values of extracted parameters

The median across subjects for different regions, showing the variation in parameters across them. The plot was not included in the main text due to failure in showing a difference across subjects and regions after the repeated measures ANOVA test. (Fig.4.3, 4.4)

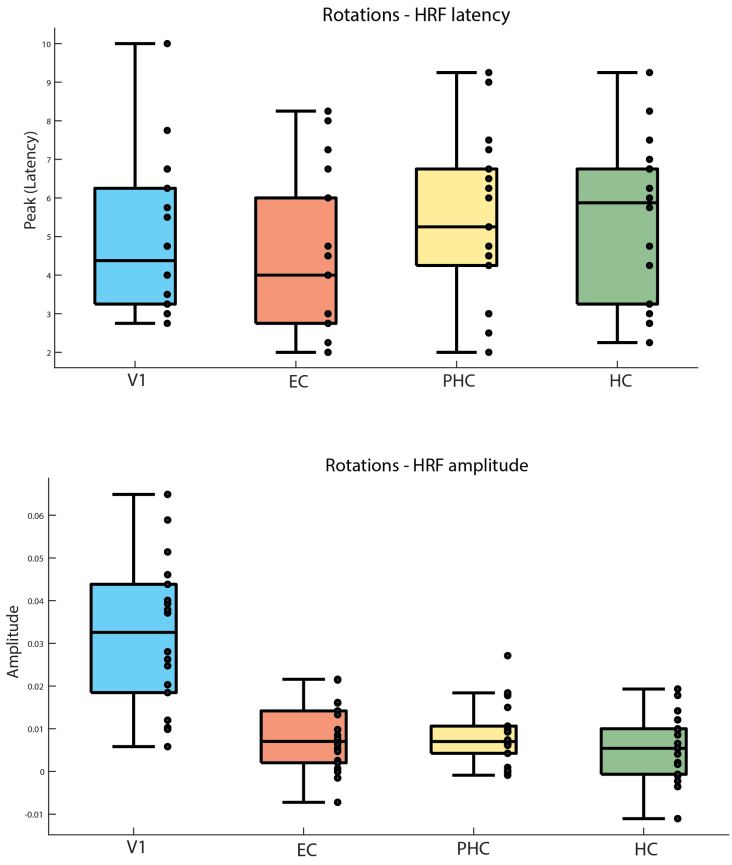


**Figure 4.4:** Rotation parameters- median values

### Limitations of parameter extraction

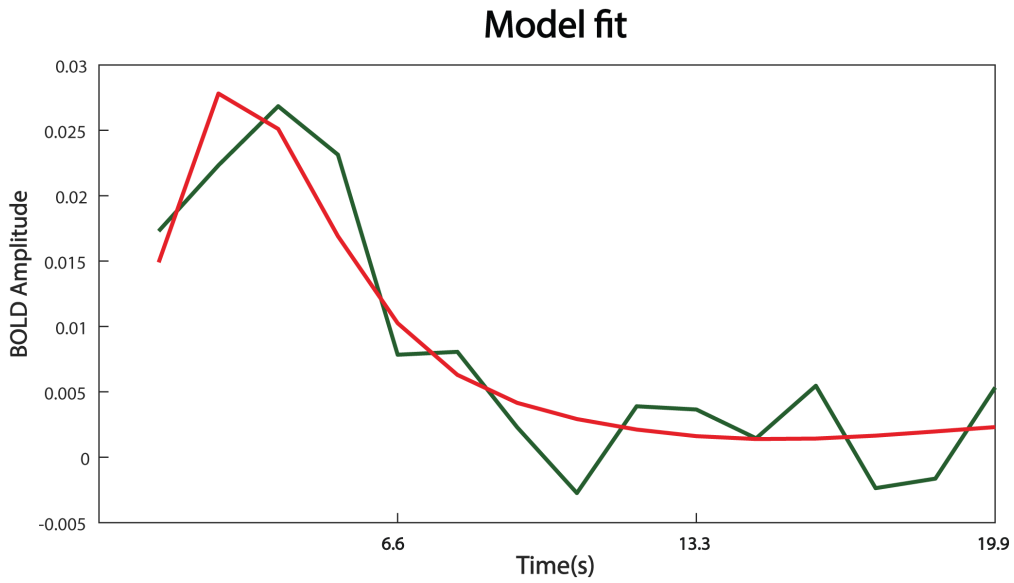


**Figure 4.5:** Parameter extraction- Limitations: The plot show the inaccuracy in the delay to peak value, selecting a kernel(red) leading to almost 2 sec inaccuracy to the actual data(green)